

# Dynamics of a Solidifying Icy Satellite Shell

J. J. Buffo<sup>1</sup>, C. R. Meyer<sup>1</sup>, and J. R. G. Parkinson<sup>2</sup>

<sup>1</sup>Thayer School of Engineering, Dartmouth College, Hanover, NH 03755, USA

<sup>2</sup>Atmospheric, Oceanic and Planetary Physics, Department of Physics, Clarendon Laboratory, University of Oxford, Parks Road, Oxford OX1 3PU, UK

## Key Points:

- The ice-ocean interfaces of icy satellites likely exist as porous layers hydraulically connected to the underlying ocean.
- The thickness of these layers is proportional to the overlying ice thickness and their upper extent coincides with the eutectic horizon.
- Thermochemical gradients within these multiphase regions could provide a metabolic energy source for any potential organisms.

---

Corresponding author: Jacob Buffo, [jacob.j.buffo@dartmouth.edu](mailto:jacob.j.buffo@dartmouth.edu)

**Abstract**

Ocean worlds have been identified as high-priority astrobiology targets due to the link between life and liquid water. Young surface terrain on many icy bodies indicates they support active geophysical cycles that may facilitate ocean-surface transport that could provide observables for upcoming missions. Accurately interpreting spacecraft observations requires constraining the relationship between ice shell characteristics and interior dynamics. On Earth, the composition, physical characteristics, and bioburden of ocean-derived ices are related to their formation history and parent fluid composition. In such systems the ice-ocean interface, which exists as a multiphase mushy layer, dictates the overlying ice's properties and evolution. Inclusion of the physics governing these boundaries is a novel strategy in modeling planetary ices, and thus far has been limited to 1D approaches. Here we present results from 2D simulations of an archetypal ice-ocean world. We track the evolution of temperature, salinity, porosity, and brine velocity within a thickening ice shell enabling us to place improved constraints on ice-ocean world properties, including: the composition of planetary ice shells, the thickness and hydraulic connectivity of ice-ocean interfaces, and heterogeneous dynamics/structures in the interfacial mushy layer. We show that stable eutectic horizons are likely a common feature of ice-ocean worlds and that ocean composition plays an important role in governing the structure and dynamics of the interface, including the formation of chemical gradient-rich regions within the mushy layer. We discuss the geophysical and astrobiological implications of our results and highlight how they can be validated by instrument specific measurements.

**Plain Language Summary**

Our solar system houses numerous ocean worlds that have the potential to harbor life. Typically these oceans reside beneath a thick global icy shell. Accordingly, much of what we know about these bodies relies on interpreting spacecraft observations of their icy exteriors. To illuminate the interior properties and dynamics of these worlds this requires an understanding of the relationship between internal processes and external observables. In ice-ocean environments the relationship between ice and ocean properties is governed by complex dynamics occurring at the ice-ocean interface. This interface is characterized by a slushy mixture of ice and brine (a mushy layer), whose physical structure, fluid flow, and chemical dynamics determine the resultant ice properties. Very few models of planetary ices include these dynamics, and so far there only exists one-dimensional models that do. Here we present the first two-dimensional model of planetary ices which includes the physics needed to accurately simulate the ice-ocean interface. We show that ice shell composition is governed by the two-dimensional dynamics of the ice-brine mushy layer, that the thickness of this layer scales directly with ice shell thickness, and that gradient rich regions in the mushy layer could provide sheltered and chemically favorable environments for organisms.

**1 Introduction**

The icy satellites of the outer solar system are some of the most enigmatic and inspirational bodies in planetary science, in large part due to their astrobiological potential (Des Marais et al., 2008; Hendrix et al., 2019; B. E. Schmidt, 2020). Ongoing geological activity and geomorphological features indicative of persistent subsurface water reservoirs suggests that these ice-ocean worlds may house aqueous environments suitable for the formation and evolution of life (Chivers et al., 2020; Hand et al., 2009; Marion et al., 2003; C. D. Parkinson et al., 2008; Porco et al., 2006; B. E. Schmidt, 2020; B. E. Schmidt et al., 2011). One of the most promising and accessible of these bodies is Europa (Hand et al., 2009, 2007; Marion et al., 2003; B. E. Schmidt, 2020). Europa likely possesses a global subsurface ocean ( $\sim 100$  km thick) underlain by a silicate mantle and roofed by a dynamic  $\sim 10$ - $30$  km thick ice shell (Schubert et al., 2004). Serpentinization reactions at the benthic water-rock interface likely provide an ongoing source of reductants to the ocean,

63 which, when coupled with surface generated oxidant delivery due to ice shell overturn (e.g.  
 64 (Allu Peddinti & McNamara, 2015; Buffo, Schmidt, Huber, & Walker, 2020; Johnson et  
 65 al., 2017)), could facilitate redox disequilibrium chemistry favorable for metabolic processes  
 66 (Vance et al., 2016). Furthermore, numerous geological features on Europa’s surface suggest  
 67 recent interaction with shallow subsurface water reservoirs (e.g. chaos (B. E. Schmidt et  
 68 al., 2011; Sotin et al., 2002) and lenticulae (Chivers et al., 2020; Manga & Michaut, 2017;  
 69 Michaut & Manga, 2014)) or even direct expression of ocean material (e.g. plumes (Jia et  
 70 al., 2018; Sparks et al., 2016) and dilational bands (Howell & Pappalardo, 2018)), providing  
 71 multiple opportunities to sample/observe the underlying ocean chemistry and any biosigna-  
 72 tures that have been entrained in the upwelling cryohydrologic system (Kargel et al., 2000;  
 73 B. E. Schmidt, 2020).

74 Europa is in good company in the outer solar system, as it is becoming increasingly  
 75 apparent that oceans are a rather ubiquitous feature of icy satellites and dwarf planets  
 76 beyond the frost line (Nimmo & Pappalardo, 2016; Buffo, 2019). Ganymede and Callisto  
 77 likely house deep subsurface oceans, potentially sandwiched between layers of high pressure  
 78 ices (Khurana et al., 1998; Vance & Brown, 2013). Enceladus’ south pole likely possesses  
 79 one of the shallowest (closest to the surface) oceans in the solar system (Nimmo, 2020), with  
 80 its iconic tiger stripes ejecting potentially endogenic materials high enough to be analyzed  
 81 by the Cassini spacecraft’s Cosmic Dust Analyzer, indicating the presence of a salty ocean  
 82 in contact with the moon’s silicate interior (Porco et al., 2006; Hansen et al., 2011; Waite  
 83 et al., 2017). If geophysical processes facilitate transport between Titan’s hydrocarbon  
 84 laden surface and its putative subsurface ocean it could create an organic rich environment  
 85 favorable for prebiotic chemistry (Fortes, 2000). Observations of active plumes and young  
 86 terrain on Triton suggest it possesses a subsurface water reservoir (McKinnon & Kirk, 2014),  
 87 and the New Horizons flyby revealed geomorphological features on both Pluto and Charon  
 88 that indicate the existence of either past or present interior oceans (Bierson et al., 2020;  
 89 Hammond et al., 2016). Here, we utilize Europa as a well studied archetype for ice-ocean  
 90 worlds, but note that our results are generally applicable and/or easily extendable to other  
 91 ice-ocean systems.

92 A crucial component to understanding the geophysics, habitability, and biosignature ex-  
 93 pression mechanisms of Europa is constraining the physicochemical evolution of its ice shell  
 94 (Allu Peddinti & McNamara, 2015; Hand et al., 2007; Kargel et al., 2000; B. E. Schmidt  
 95 et al., n.d.; B. E. Schmidt, 2020; Vance et al., 2016). As the barrier to and facilitator of  
 96 ocean-surface interaction the material and transport properties of the ice shell will govern  
 97 the geomorphological evolution of Europa’s surface, the entrainment of ocean-derived im-  
 98 purities in the shell, and the chemistry of the underlying ocean (Buffo, Schmidt, Huber, &  
 99 Walker, 2020; Vance et al., 2016). Moreover, the ice shell will act as the primary observa-  
 100 tional medium for upcoming spacecraft missions (e.g. Europa Clipper, JUICE) (Pappalardo  
 101 et al., 2017; Grasset et al., 2013), which makes quantifying the relationship between empir-  
 102 ical ice shell properties and interior processes an imperative for optimal data interpretation  
 103 and synthesis (e.g. (Kalousová et al., 2017)). However, while numerous investigations  
 104 have emphasized the importance of physicochemical heterogeneities within and the mate-  
 105 rial transport capabilities of the ice shell to both geophysical and potential astrobiological  
 106 processes on Europa (e.g. (Barr & McKinnon, 2007; Han & Showman, 2005; Johnson et  
 107 al., 2017; Kargel et al., 2000)) the structural and compositional details of the shell remain  
 108 largely unconstrained. It is widely believed that Europa’s ice shell is in a stagnant lid ther-  
 109 mal regime; suggesting the presence of a thin ( $\sim 3\text{-}5$  km), brittle, ice lithosphere overlying a  
 110 thicker ( $\sim 10\text{-}30$  km), ductile, isothermal icy mantle undergoing solid state convection (Barr  
 111 & McKinnon, 2007; McKinnon, 1999; Schubert et al., 2004). Additionally, a number of in-  
 112 vestigations have highlighted likely trends in non-ice material distribution within Europa’s  
 113 ice shell (e.g. (Buffo, Schmidt, Huber, & Walker, 2020; Kargel et al., 2000; Zolotov &  
 114 Kargel, 2009)), with higher impurity entrainment in the shallow shell (Zolotov & Kargel,  
 115 2009) and around intrusive hydrological features within the shell (Buffo, Schmidt, Huber, &  
 116 Walker, 2020) and more efficient solute rejection as the ice shell thickened and ice-ocean in-

117 terfacial growth rates slowed. Nevertheless, only Buffo, Schmidt, Huber, and Walker (2020)  
118 provide quantitative estimates for the compositional profile of the shell and themselves rec-  
119 ognize the limitations of a one-dimensional model in an inherently multidimensional system  
120 (Buffo, Schmidt, Huber, & Meyer, 2020).

121 Multiphase reactive porous media, or ‘mushy layers’, play a fundamental and dispro-  
122 portionate role in the dynamics and evolution of both biogeochemical and geophysical systems  
123 (e.g. (Loose et al., 2011; Steefel et al., 2005; Tedesco & Vichi, 2014)). The ice-ocean  
124 layers of icy worlds, including Earth, are no exception. The complex reactive transport pro-  
125 cesses occurring near ice-ocean interfaces governs heat and mass transport between the two  
126 reservoirs and dictates the physicochemical properties of and impurity entrainment in the  
127 overlying ice (Buffo, Schmidt, Huber, & Walker, 2020; Hunke et al., 2011; Thomas & Dieck-  
128 mann, 2008). With direct implications for ice rheology (Assur, 1958; Durham et al., 2005),  
129 buoyancy (Han & Showman, 2005), eutectic point (McCarthy et al., 2011, 2007), bioburden  
130 (Santibáñez et al., 2019; Buffo, 2019; Brown et al., 2020), and conductivity (Kalousová et al.,  
131 2017) constraining the dynamics of ice-ocean/brine interfaces can improve our fundamental  
132 understanding of icy world geophysics and aid in spacecraft data analysis/interpretation  
133 (e.g. ice penetrating radar (Schroeder et al., 2016)). Furthermore, the ice-ocean interface of  
134 terrestrial ices provides a gradient rich substrate where both micro- and macro-fauna thrive  
135 in appreciable densities (Ackley & Sullivan, 1994; Daly et al., 2013; Spindler, 1994; Thomas  
136 & Dieckmann, 2003). It has been suggested that the thick ice shells of low-gravity moons  
137 will support thicker multiphase boundary layers at the ice-ocean interface (on the order of  
138 meters to tens of meters), as this layer’s thickness is inversely proportional to the interfacial  
139 thermal gradient (Buffo, Schmidt, Huber, & Meyer, 2020). This is supported by observations  
140 of columnar sea ice formed beneath the Ross Ice Shelf, which exhibited brine channels, high  
141 impurity entrainment, and hydraulic connectivity to the underlying ocean throughout the  
142 bottom 6 m of ice (Zotikov et al., 1980). Convective overturn of high salinity brine in these  
143 porous boundary layers leads to the formation of heterogenous channel structures within the  
144 ice matrix (Cottier et al., 1999; Wells et al., 2011; Wettlaufer et al., 1997) and can produce  
145 brinicles that extend into the underlying ocean from the basal ice surface (Cartwright et al.,  
146 2013). As cold, saline brine is convected out of the mushy layer in localized downwelling  
147 plumes it acts as a heat sink for the surrounding seawater, in some cases depressing the local  
148 temperature enough that an ice membrane forms around the saline fluid (e.g. (Mahadevan,  
149 2017)). These tubular ice membranes produce regions with exceptionally high thermal and  
150 chemical gradients that could serve as an oasis for biology, akin to terrestrial hydrothermal  
151 and chemical garden systems (Cartwright et al., 2013; Vance et al., 2019). This possibility  
152 is strengthened by the fact that the ice-ocean interface will be the site of oxidant delivery to  
153 the ocean, providing a redox boon for any potential organisms (Allu Peddinti & McNamara,  
154 2015; Vance et al., 2016).

155 Understanding the structure and dynamics of the ice-ocean interface of icy worlds has  
156 both geophysical and astrobiological implications (Buffo, Schmidt, Huber, & Meyer, 2020;  
157 Buffo, Schmidt, Huber, & Walker, 2020). It is a mandatory port of call for ocean-surface  
158 interaction, a core-mantle boundary in the cryospheric system that could facilitate regional  
159 geomorphological heterogeneities, and likely one of the most habitable environments on high  
160 priority astrobiology targets. Here, we simulate the multiphase two-dimensional evolution of  
161 Europa’s ice-ocean interface. We provide improved constraints on the compositional profile  
162 of the growing ice shell and the relationship between ice-ocean interface thermal gradient and  
163 impurity entrainment. We show that the multiphase ice-ocean boundary layer thickens as  
164 Europa’s ice shell thickens and interfacial thermal gradients decrease. Additionally, we show  
165 that brinicles are a likely byproduct of the convective overturn of brine in the porous basal  
166 ice layer. Finally, we discuss how our estimations of ice shell structure and composition can  
167 be utilized to improve geophysical models, constrain the habitability, and aid in spacecraft  
168 mission planning and data analysis of Europa and other icy worlds.

## 2 Methods

To simulate the two-dimensional evolution of Europa’s ice-ocean interface we use the reactive porous media model SOFTBALL: Solidification, Flow, and Thermodynamics in Binary ALloys. First introduced in J. R. G. Parkinson, Martin, Wells, and Katz (2020), SOFTBALL is an open source code capable of efficiently simulating the phase evolution, heat transport, and mass transport in mushy layers. The code has been tested extensively (cf. (J. R. G. Parkinson, 2019; J. R. G. Parkinson, Martin, Wells, & Katz, 2020; Wells et al., 2019)), and we provide an additional validation of the model’s ability to reproduce the compositional and structural properties of terrestrial sea ice in the Supplementary Material.

The equations governing the evolution of ice-ocean interfaces are well documented in the literature (e.g. (Feltham et al., 2006; Hunke et al., 2011; Worster, 1997)). Employing the Boussinesq approximation and assuming no phase change driven flow ( $\rho_{br}=\rho_i$ , where  $\rho_{br}$  is brine density, and  $\rho_i$  is ice density), conservation of mass in a reactive porous media requires

$$\nabla \cdot \mathbf{q} = 0 \quad (1)$$

where  $\mathbf{q} = (u, v)$  is the two-dimensional Darcy velocity. Fluid flow is governed by the incompressible form of Darcy’s law

$$\mathbf{q} = -\frac{\Pi}{\mu} (\nabla p + \rho_{br} \mathbf{g}) \quad (2)$$

where  $\Pi$  is permeability (typically a function of porosity, here we utilize the Kozeny-Carman relationship given in J. R. G. Parkinson, Martin, Wells, and Katz (2020), see Eq. 6),  $\mu$  is dynamic viscosity of the brine,  $p$  is dynamic pressure, and  $\mathbf{g}$  is gravity. Conservation of energy is given by

$$\bar{\rho} c \frac{\partial T}{\partial t} = -\rho_{br} c_{br} \mathbf{q} \cdot \nabla T + \nabla \cdot (\bar{k} \nabla T) - \rho_i L \frac{\partial \phi}{\partial t} \quad (3)$$

where  $c$  is specific heat,  $T$  is temperature,  $k$  is thermal conductivity, and  $L$  is the latent heat of the water-ice phase transition. Quantities with overbars are volume averaged quantities (i.e.  $\bar{k} = \phi k_{br} + (1 - \phi) k_i$ , where  $\phi$  is liquid fraction (porosity)). This equation accounts for heat transport via advection and diffusion as well as the generation/usage of heat due to freezing/melting. Similarly, the conservation of salt is given by

$$\phi \frac{\partial C}{\partial t} = -\mathbf{q} \cdot \nabla C + \nabla \cdot (D \nabla C) - \frac{\rho_i}{\rho_{br}} C \frac{\partial \phi}{\partial t} \quad (4)$$

where  $C$  is brine concentration, and  $D$  is the diffusion coefficient of the solute. This allows for evolution of the brine phase via advection, molecular diffusion, and concentration/dilution caused by freezing/melting of ice. The system of Equations 1-4 can be closed by assuming that the system is in local thermodynamic equilibrium and that the liquidus curve is a function of the brine concentration

$$T = T_L(C) = T_m - mC \quad (5)$$

where  $T_L$  is the liquidus temperature,  $T_m$  is the freezing temperature of pure water, and  $m$  is a solutal freezing point depression coefficient with units of  $\text{K kg g}^{-1}$  (equivalently,  $\text{K ppt}^{-1}$ ).

Here we simulate the top-down solidification of a hypothetical European ocean using the initial and boundary conditions presented in Figure 1 and the physical parameter values given in Table 1. We have chosen to use an ocean with a salinity of 35 ppt and linear liquidus

205 slope of -0.048 K/ppt as this lies comfortably within the range of predicted European ocean  
 206 concentrations (Hand & Chyba, 2007; Zolotov & Shock, 2001) and compositions (Trumbo  
 207 et al., 2019; Zolotov & Shock, 2001). Simulations are initiated as a completely fluid filled  
 208 domain subject to an undercooled upper boundary ( $T_s=100$  K) which induces the formation  
 209 of an ice shell. Throughout the simulation SOFTBALL tracks the evolving temperature  
 210 ( $T$ ), bulk salinity ( $C$ ), porosity ( $\phi$ ), and velocity ( $u, v$ ) within the system. By assuming  
 211 the domain exists as a thin Hele-Shaw cell a finite fluid permeability (J. R. G. Parkinson,  
 212 Martin, Wells, & Katz, 2020)

$$\Pi(\phi) = \left\{ \frac{12K_0}{d^2} + \left[ \frac{\phi^3}{(1-\phi)^2} \right]^{-1} \right\}^{-1} \quad (6)$$

213 allows us to solve for flow throughout the entire domain using Darcy's law (Eq. 2).  $K_0$  is  
 214 a permeability factor and  $d$  is the Hele-Shaw cell spacing. This approach optimizes com-  
 215 putation speed as the Darcy equation is simpler to solve than the full Navier-Stokes and  
 216 restricting flow in the underlying fluid permits the use of larger CFL-limited time steps.  
 217 Additionally, it limits phase boundary effects (removing the need to define interfacial condi-  
 218 tions between the fluid and porous regions, e.g. multiple domain Stokes-Darcy approaches  
 219 (Le Bars & Worster, 2006)) while ensuring the underlying fluid has an amplified permeabil-  
 220 ity such that it will not artificially impact the evolution of the overlying porous region. This  
 221 is a common approach to simulating mushy layers (e.g. (J. R. G. Parkinson, Martin, Wells,  
 222 & Katz, 2020; Katz & Worster, 2008)).

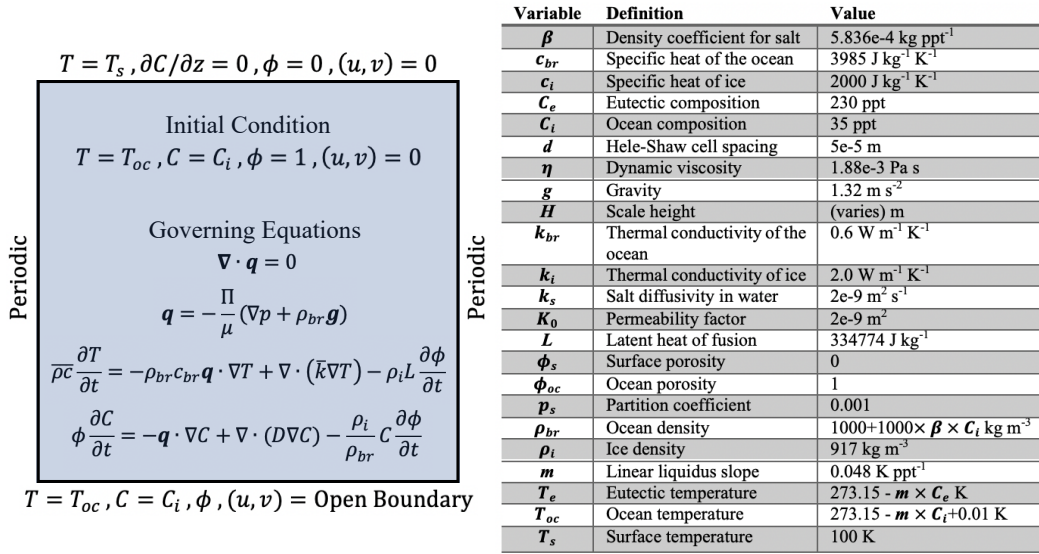


**Figure 1.** (Left) – Initial and boundary conditions utilized in the top-down solidification simulations. **Table 1.** (Right) – Variables used by the SOFTBALL code. The scale height,  $H$ , is used to define the simulation domain size and nondimensionalize the system.

### 223 3 Results

#### 224 3.1 Bulk Salinity of Europa's Ice Shell and its Relation to Thermal Gradient

225 To constrain the bulk salinity of Europa's ice shell we simulated the top-down solidi-  
 226 fication of the shallow shell (0-1.1 km) using twelve different domain sizes and resolutions.

227 The consistency of results across a range of resolutions further validates the model’s ability  
 228 to accurately capture the continuum mechanics that govern the system, even in simulations  
 229 where small scale heterogeneities such as brine channels are not explicitly resolved. An  
 230 example of the two-dimensional bulk salinity and porosity profiles produced by such a run  
 231 can be seen in Figure 2. This particular simulation was conducted using a 20 m by 20 m  
 232 domain at a resolution of 3.9 cm (resolution results from a 512 x 512 grid). Both fossilized  
 233 and active high salinity regions can be seen throughout the thickness of the forming ice shell,  
 234 suggesting a heterogeneous and appreciable distribution of salt within the ice. It is impor-  
 235 tant to note that there may be additional substructure within these regions not captured at  
 236 the current simulation resolution (brine channels in natural sea ice on Earth are typically  
 237  $\sim 1\text{-}3$  mm in diameter), however the dendritic structure and density distribution (channel  
 238 collapse as the ice thickens) of the high salinity regions matches both observations and the-  
 239 oretical predictions of ice-ocean systems (Rees Jones & Worster, 2013; Wells et al., 2011,  
 240 2019; Worster & Rees Jones, 2015). Also apparent is the existence of a thin (in relation to  
 241 the overall ice thickness), dynamic mushy layer at the ice-ocean interface. The convective  
 242 overturn of brine within this layer (Figure 2b) is responsible for the desalination of, and thus  
 243 the level of ocean-derived material entrainment in, the ice shell (Buffo, Schmidt, Huber, &  
 244 Walker, 2020; Wells et al., 2019; Wettlaufer et al., 1997; Worster, 1997). Darcy velocities  
 245 within the mushy layer range from  $\sim 10^{-11}$  m/s near the ice-mush interface where porosity  
 246 approaches zero and  $\sim 10^{-6}$  m/s in the downwelling saline plumes.

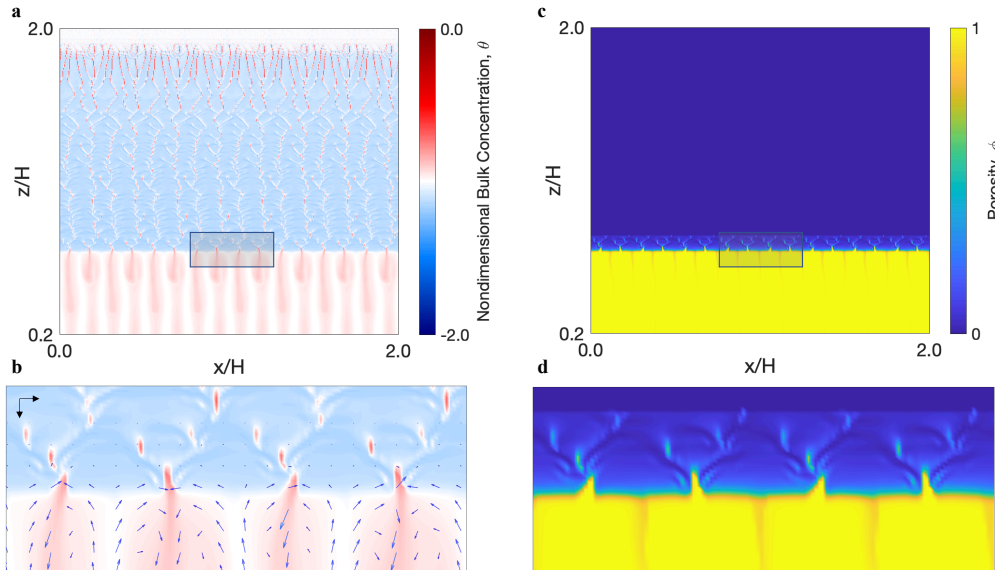


**Figure 2.** The compositional (bulk salinity) and structural (porosity) profile in Europa’s growing ice shell. **a)** Two-dimensional nondimensionalized bulk salinity profile using a scale height,  $H$ , of 10 m (domain size: 18m x 20m). Where nondimensional bulk salinity,  $\theta = \frac{C-C_e}{C_e-C_i}$ . Fossilized high salinity regions can be seen in the upper ice and dense, high salinity plumes can be seen emanating from the ice-ocean interface. **b)** Magnified view of the shaded box in panel (a), with velocity vectors included, showing the convective overturn of brine within the interfacial mushy layer. For scale, black arrows in the top left have lengths that represent Darcy velocities of  $10^{-6}$  m/s **c)** Two-dimensional porosity profile for the same region depicted in panel (a). **d)** Magnified view of the shaded box in panel (c). Low porosity brine channels are associated with high salinity downwellings.

247 To investigate how the ice shell composition varies with depth we horizontally average  
 248 the bulk salinity of each two-dimensional run and plot it against it's corresponding location  
 249 within the shell (Figure 3a-c). It can be shown that the temperature profile in the forming  
 250 ice varies negligibly from a simple conductive (linear) profile (See Supplementary Section  
 251 S2), and thus the ice-ocean interface thermal gradient is well represented by

$$\frac{\partial T}{\partial z} = \frac{T_{oc} - T_s}{H_{shell}}, \quad (7)$$

252 where  $T_{oc}$  is ocean temperature,  $T_s$  is surface temperature, and  $H_{shell}$  is the depth of the  
 253 ice-ocean interface from the surface. Plots of bulk salinity as a function of interfacial thermal  
 254 gradient can be found in Figure 3d-f. The functional form of the best fit lines closely follow  
 255 the analytical solutions derived by Buffo, Schmidt, Huber, and Walker (2020) (Equations 26  
 256 & 27 of their manuscript) for the compositional evolution of a simplified ice-ocean system.  
 257 Here we implement a Levenberg-Marquardt algorithm to relate bulk salinity and depth  
 258 within the ice shell using the equation

$$C(z) = a + \frac{b}{c-z} [1 - d \exp(-fz)] \quad (8)$$

259 where  $C$  is bulk salinity,  $z$  is depth within the shell, and  $a$ ,  $b$ ,  $c$ ,  $d$ , and  $f$  are constant  
 260 coefficients that account for stretches and translations. Similarly, we relate bulk salinity to  
 261 thermal gradient using the equation

$$C \left( \frac{\partial T}{\partial z} \right) = a + \frac{b \left( \frac{\partial T}{\partial z} + c \right)}{\left( d + f \frac{\partial T}{\partial z} \right)} \left[ 1 - h \exp \left( \frac{-j}{\frac{\partial T}{\partial z}} \right) \right], \quad (9)$$

262 where  $a$ ,  $b$ ,  $c$ ,  $d$ ,  $f$ ,  $h$ , and  $j$  are constant coefficients that account for stretches and transla-  
 263 tions.

264 The simulated bulk salinity values are well approximated by the functional forms of  
 265 Equation 8 & 9, and exhibit a number of important trends and features predicted by earlier  
 266 studies (e.g. (Buffo, Schmidt, Huber, & Walker, 2020)). These include a trend toward com-  
 267 positional homogeneity as the ice shell thickens and interfacial thermal gradients decrease; a  
 268 nonzero lower limit for entrainment rate (0.984 ppt as  $z \rightarrow \infty$  and 1.448 ppt as  $\partial T/\partial z \rightarrow 0$ ),  
 269 as predicted by Equations 8 & 9, respectively); one hundred percent salt retention when ice  
 270 forms under large thermal gradients (representative of rapid freezing); and the existence of  
 271 transitional regimes in mushy layer dynamics (evidenced by the ‘shoulder’ region of Figure  
 272 3e). These properties and their implications for the geophysics and astrobiology of Europa  
 273 and other ice-ocean worlds are discussed in Section 4.

### 274 3.2 Ice-Ocean Interface Mushy Layer Thickness

275 The porous region near the ice-ocean interface (e.g. Figure 2d) plays an important role  
 276 in governing the properties and evolution of the ice shell. This dynamic region dictates the  
 277 chemical composition and physical structure of forming ice, governs heat and solute trans-  
 278 port between the ocean and ice shell reservoirs, and determines the hydraulic connectivity  
 279 of the deep ice shell. Studies suggest that the properties of this layer are dynamic and evolve  
 280 as the overlying ice cover thickens and interfacial thermal gradients decrease (e.g. (Buffo,  
 281 Schmidt, Huber, & Meyer, 2020)). Furthermore, the environmental parameters (e.g. grav-  
 282 ity, ocean composition) of a given system will impact the layer's structure, suggesting that  
 283 a diverse array of deep ice shell environments exist across the solar system and throughout  
 284 individual ice-ocean world's lifetimes.

285 To constrain the evolving thickness of Europa's ice-ocean interface mushy layer we  
 286 slightly modified the boundary conditions presented in Figure 1 such that the upper ther-  
 287 mal boundary was governed by a Neumann (gradient/flux) boundary condition ( $\partial T/\partial z =$   
 288  $(T_{oc} - T_s)/H_{shell}$ ) and carried out high resolution, top-down solidification simulations for

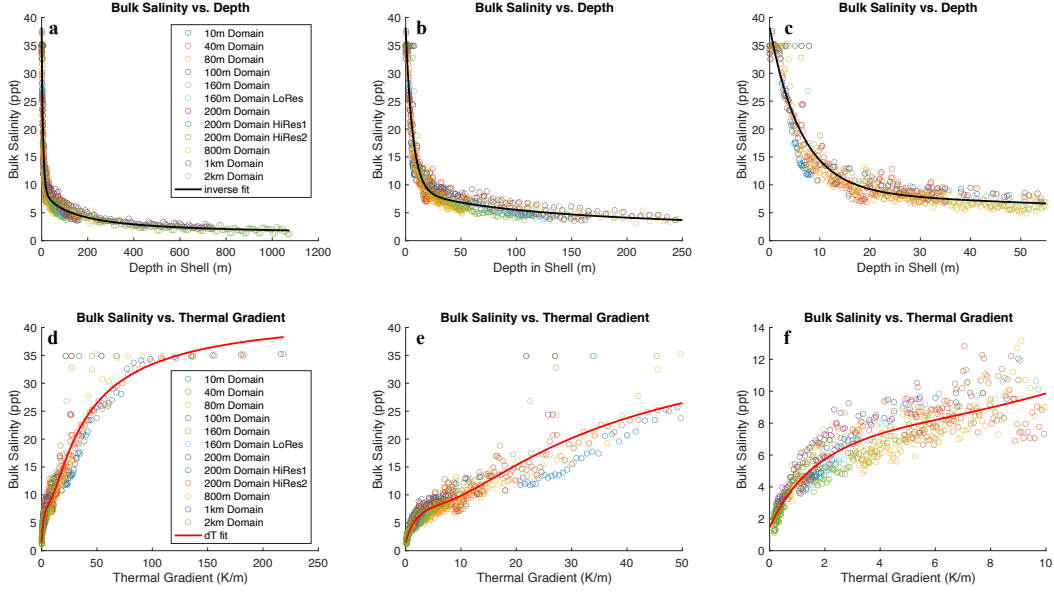


**Figure 3.** Bulk salinity characteristics of Europa’s ice shell for a 35 ppt ocean. **a-c)** Bulk salinity variation with depth in the shell. High salinity values near the surface quickly decrease with depth and asymptotically approach a lower limit of 0.984 ppt, according to the best fit line of Equation 8 (coefficients:  $a=0.984$ ,  $b=-1014$ ,  $c=-123.4$ ,  $d=-3.529$ ,  $f=0.1529$ ). **d-f)** Bulk salinity variation with ice-ocean interface thermal gradient (assuming a conductive profile in the overlying ice shell). At large thermal gradients ( $>100$  K/m) all salt is trapped within the ice. There is a prominent ‘shoulder’ region between 3-10 K/m that is captured well by the fit line of Equation 9 (coefficients:  $a=7.864$ ,  $b=-2576$ ,  $c=-5.148$ ,  $d=-2067$ ,  $f=-869.2$ ,  $h=-10.9$ ,  $j=27.2$ ). This regime could be indicative of a transition between dominant desalination mechanisms in the mushy layer (Buffo, Schmidt, Huber, & Walker, 2020; Buffo, Schmidt, Huber, & Meyer, 2020). (Note: Two data points with bulk salinity  $>35$  ppt visible in panels (a-c) do not appear in panels (d-f) as they are the result of interfacial thermal gradients which exceeded 250 K/m. These results negligibly affect the fit lines of Equations 8 and 9 while highlighting the difficulty of accurately simulating extreme thermal environments, as we expect these values to be 35 ppt)

289 descending depths within the shell ( $H_{shell} = 0$  m, 25 m, 50 m, 100 m, 250 m, 500 m, and  
 290 1000 m). Porosity profiles during three of these runs can be seen in Figure 4. Periodically  
 291 during these runs the porosity profile was horizontally averaged and the region satisfied by  
 292  $1e-5 < \phi < 0.95$  was measured, giving the mushy layer thickness. These bounds were selected  
 293 in lieu of  $0 < \phi < 1$  to avoid measuring any residual low porosity regions in the upper  
 294 ice shell and any high porosity structures extending from the ice-ocean interface (e.g. brini-  
 295 cles - the focus of Section 3.3). The relationship between ice-ocean interface mushy layer  
 296 thickness and ice shell thickness can be seen in Figure 5a. Figure 5b shows the fraction of  
 297 the ice shell occupied by the mushy layer and its relationship to ice shell thickness. The  
 298 increase in mushy layer thickness with growing ice shell thickness is well fit by the analytical  
 299 solution derived by (Buffo, Schmidt, Huber, & Meyer, 2020), (modified from Equation 25  
 300 of (Buffo, Schmidt, Huber, & Meyer, 2020)):

$$h_{ML} = aH_{shell} \left( 1 + \sqrt{1 - \frac{b}{H_{shell}} - \frac{c}{H_{shell}^2}} \right) \quad (10)$$

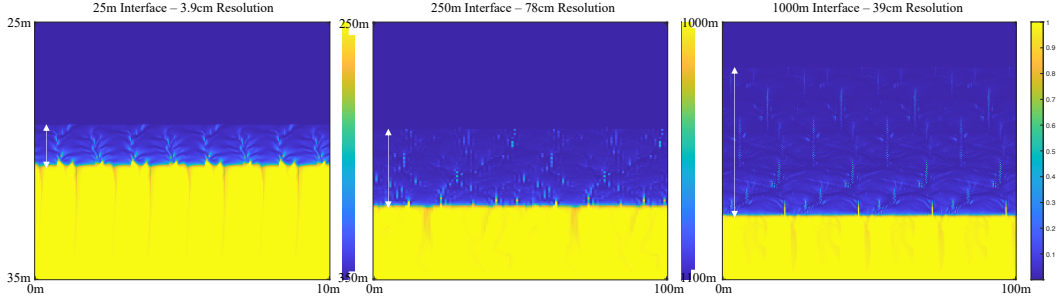


**Figure 4.** Thickness and structure of the ice-ocean interface mushy layer at various depths within the ice shell. The mushy layer thickness increases as the ice shell thickens, consistent with previous observations and theory (Buffo, Schmidt, Huber, & Meyer, 2020; Wells et al., 2011). The majority of fluid motion is concentrated in a high porosity region near the base of the mushy layer (e.g. Figure 2b), resulting in a ‘stagnant’ region with decreased fluid flow underlain by a thin convecting boundary layer. This was predicted theoretically by Worster (1991) for systems with large mush Rayleigh numbers, which is the case for the mushy layers considered here (see supplementary section S3). White arrows demarcate the horizontally averaged mushy layer thickness. (Note: The left image depicts a 10 m x 10 m domain while the center and right images depict a 100 m x 100 m domain.)

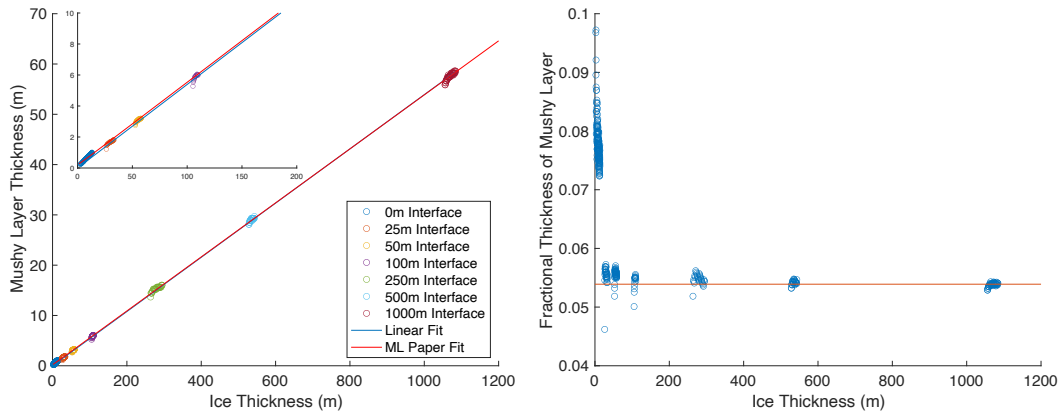


**Figure 5.** Ice-ocean interface mushy layer thickness and its relationship to ice shell thickness. **(Left)** Mushy layer thicknesses recorded during seven simulations, each initiated with a different ice-ocean interface position (overlying ice shell thickness,  $H_{shell}$ ). The relationship between mushy layer thickness and ice shell thickness is well captured by the fit line of Equation 10, here ‘ML Paper Fit’. A simple linear relationship also closely matches the data, evidenced by its overlap with the fit line of Equation 10 until the plot is magnified. (‘ML Paper Fit’ coefficients:  $a=0.02685$ ,  $b=-11.64$ ,  $c=-62.28$ ; linear relationship= $0.0539$ ). Inset – magnified view of the shallow ice shell region (0-200 m). **(Right)** The fractional percentage of the ice shell occupied by the mushy layer. The red line corresponds to the linear fit trend of 0.0539.

301 where  $h_{ML}$  is mushy layer thickness,  $H_{shell}$  is ice shell thickness, and  $a$ ,  $b$ , and  $c$  are constants  
 302 that allow for translations and stretches. The relationship between mushy layer thickness  
 303 and ice shell thickness is also well approximated by a simple linear trend (relationship

coefficient = 0.0539). This suggests that accretionary regions of Europa’s ice shell likely possess a substantial multiphase ice-ocean boundary layer that occupies as much as 5% of the ice shell thickness. Notably, the linear relationship coefficient closely matches the eutectic horizon predicted by assuming a conductive (linear) thermal profile within the ice shell ( $h_{eut} = \frac{T_{oc} - T_e}{T_{oc} - T_s} = 0.0548$ ). While slightly overestimating the mushy layer’s thickness, eutectic horizons likely provide an exceptional first order estimate of ice shell hydrological structure. This has important implications for regional and global geophysical processes, ocean-derived material entrainment in the shell, and Europa’s potential habitability (further discussed in Section 4).

### 3.3 Fine Scale Heterogeneities and Brinicle Formation

The fine scale structure in the multiphase region near the ice-ocean interface (e.g. Figure 2) supports thermochemical gradients that when combined with the porous nature of the ice-brine matrix could provide an ample substrate for any potential organisms. Vance et al. (2019) suggested that brinicles (hollow tubes of ice formed around downwelling brine plumes) could form at the ice-ocean interfaces of icy worlds and result in chemical garden like structures. Similar to the hydrothermally formed chemical garden systems at Earth’s seafloor, an oasis for life (Barge et al., 2015; Cartwright et al., 2002), brinicles and the mushy layer they grow from could provide a gradient rich habitat for an inverted benthic community (Cartwright et al., 2013).

To investigate the physicochemical properties of brinicles on Europa we performed high resolution simulations of the ice-ocean interface for a number of overlying ice shell thicknesses (similar to Section 3.2). The resulting porosity, brine salinity, and salinity gradient profiles for three such simulations are depicted in Figure 6. Brinicle structures can be seen extending from the mushy layer in all three cases (left column of Figure 6). The size of the brinicle structures increases with ice shell thickness. This is consistent with the convective patterns in a thickening mushy layer, where downwellings drain an increasingly large region of the mushy layer as brine channel spacing increases. Brinicle size may also be affected by their longevity. The ice-ocean interface is quite dynamic and brinicle structures grow and disappear repeatedly during simulations. The timescale over which this cycling occurs increases with depth, suggesting a thicker ice shell may promote the formation of larger and more stable ‘brinicle gardens’. The lifetimes of brinicles at an ice-ocean interface depth of 10 m, 50 m, and 1000 m are on the order of hours, days, and years, respectively. Salinity gradients are highest near brine channels within the mushy layer and at the edges of downwelling high salinity plumes. While the brinicle structures themselves do not house large salinity gradients, they form directly adjacent to regions that do (downwelling plumes). This is expected as brinicle formation is a result of the difference between thermal and molecular diffusivity in the system (Cartwright et al., 2013).

It is important to note, however, that brinicles on Earth only occur near land, in sheltered water where currents are low. Stronger currents induce turbulent mixing near the ice-ocean interface, dissipating the downwelling plumes and preventing brinicle formation. Given the substantial latitudinal currents predicted for icy satellites in the outer solar system (e.g. (Soderlund et al., 2014; Soderlund, 2019)) it is quite possible that brinicles may not be able to form. Conversely, the gradient rich brine channels within the mushy layer are protected from the underlying shear flow by the surrounding ice matrix. This suggests a putative ice-ocean interface habitat more akin to the terrestrial infaunal benthos rather than the extensional structures of chemical gardens. The importance of the ice-ocean interface as a potentially habitable environment on icy worlds as well as potential limitations of the current model in simulating brinicle geometry and evolution is discussed in Section 4 and Supplementary Section S4, respectively.

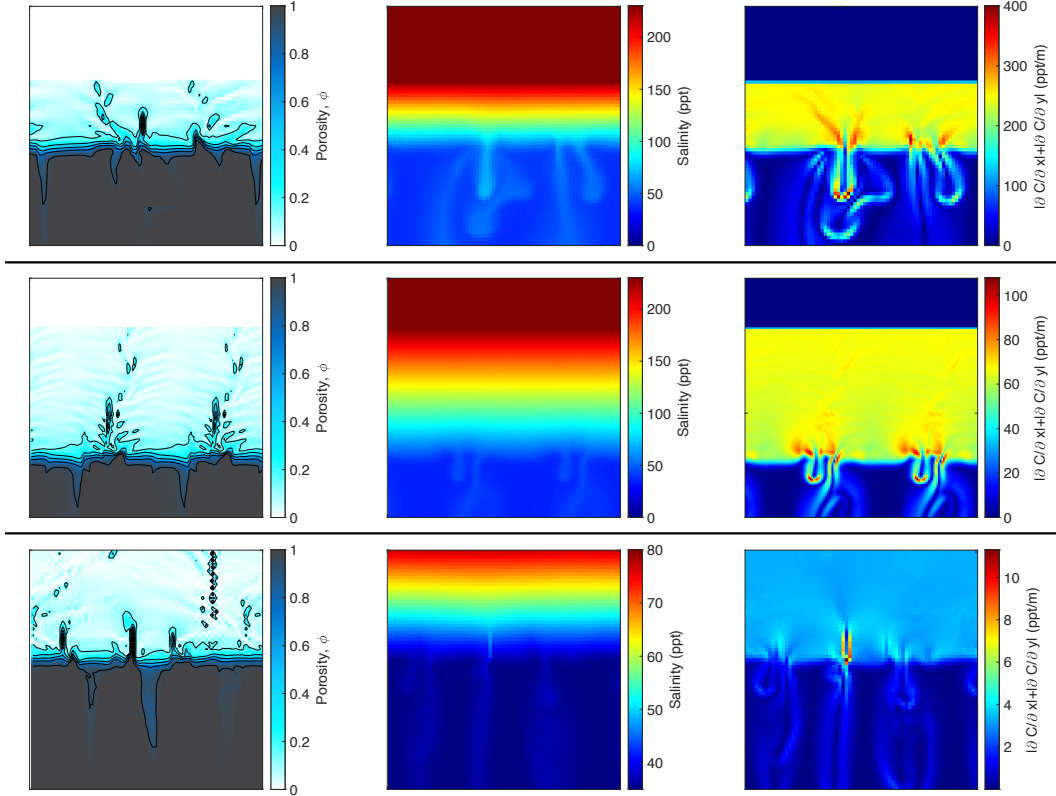


**Figure 6.** The physicochemical properties of brinicles on Europa. **(Top-Bottom)** Simulation results when the ice-ocean interface is at a depth of Top – 11 m (2.75 m x 2.75 m grid), Middle – 56 m (5.5 m x 5.5 m grid), and Bottom – 1084 m (27.5 m x 27.5 m grid). **(Left-Right)** Porosity (contours demarcate porosities of 0.15 to 0.95 in increments of 0.2), brine salinity, and absolute salinity gradient ( $|\partial C/\partial x| + |\partial C/\partial y|$ ) profiles during the simulations. (Note: the scale of the color bars differs between some of the images so as to highlight gradients within individual images. Additionally, these images have been extracted from simulations spanning much larger domains, ensuring the mushy layer is not impacted by edge effects.)

353

#### 4 Discussion

354

355

356

357

358

359

The ability to simulate, at high resolution, the two-dimensional evolution of Europa’s ice-ocean interface offers insight into the important role this boundary plays on icy worlds. A few examples are: the distribution of ocean-derived material within the ice shell; the relationship between impurity entrainment and ice-ocean interfacial thermal gradient; the physicochemical structure of the ice-ocean interface; and the potential implications the ice-ocean interface may have on habitability and geophysical processes.

360

361

362

363

364

365

366

367

Our work corroborates the work of Buffo, Schmidt, Huber, and Walker (2020) who implemented a one-dimensional reactive transport model to predict the bulk salinity profile of Europa’s forming ice shell and the evolution of hydrological structures within the shell. The functional relationship between bulk salinity and depth within the ice shell derived by Buffo, Schmidt, Huber, and Walker (2020) captures the structure of the bulk salinity profile simulated in this study (Figure 3a-c). In the shallow shell substantial amounts of salt are retained in the forming ice, but as the ice shell thickens salt is more efficiently drained from the mushy layer and bulk salinity asymptotically approaches a nonzero lower limit. This

368 lower limit is governed by the permeability of the mushy layer at low porosities. While an  
 369 extremely important value in predicting the dynamics of the ice-ocean interface, it is not well  
 370 constrained (Buffo, Schmidt, Huber, & Walker, 2020; Golden et al., 1998, 2007) and remains  
 371 a contentious topic and active field of research (Freitag & Eicken, 2003; McCarthy et al.,  
 372 2013; Petrich et al., 2006). Similarly, our results show that at high thermal gradients ( $>100$   
 373 K/m) ice effectively traps all of the salt from the parent liquid (i.e. freezing is too rapid  
 374 for salts to be expelled from the ice). Our results demonstrating the relationship between  
 375 salt entrainment and interfacial thermal gradient (Figure 3d-f) are an improvement on the  
 376 results of Buffo, Schmidt, Huber, and Walker (2020) whose one-dimensional model struggled  
 377 with stability issues under thermal gradients  $>20$  K/m.

378 We have shown that there exists a distinct and quantifiable relationship between the  
 379 thermochemical environment of the ice-ocean interface at the time of solidification and the  
 380 properties of the ice that forms. With the likelihood of ongoing hydrological activity within  
 381 Europa's ice shell in the form of lenses (B. E. Schmidt et al., 2011; Spaun et al., 1998), sills  
 382 (Chivers et al., 2020; Craft et al., 2016; Manga & Michaut, 2017; Michaut & Manga, 2014),  
 383 dikes, fractures (Dombard et al., 2013; Rudolph & Manga, 2009; Walker et al., 2014), and  
 384 plumes (Jia et al., 2018; Sparks et al., 2016) understanding the characteristics of ice formed  
 385 in an array of thermal environments is imperative in constraining the mechanical, dielectric,  
 386 and eutectic properties of refrozen features. The presence of salt alters the rheological  
 387 properties of ice (Assur, 1958; Durham et al., 2005; McCarthy et al., 2011) and could  
 388 facilitate the reactivation of fractures as well as the dynamics of solid-state convection in  
 389 the ductile portion of the ice shell (e.g. Buffo, Schmidt, Huber, and Walker (2020)). Shallow  
 390 lenses within the shell can be drastically affected by the dynamics of ice formation and salt  
 391 entrainment/rejection. Separated from the underlying ocean, progressive freezeout of these  
 392 features results in concentration of the residual brine, depressing the freezing point of the  
 393 fluid, increasing the lens' longevity, and potentially resulting in the precipitation of salt  
 394 hydrate layers when the reservoir reaches saturation (Buffo, Schmidt, Huber, & Walker,  
 395 2020; Chivers et al., 2020). Ice penetrating radar observations depend critically on the  
 396 dielectric properties of the ice shell (Di Paolo et al., 2016; Kalousová et al., 2017; Moore,  
 397 2000), thus detecting and distinguishing features within the ice shell as well as the ice-  
 398 ocean interface relies on our understanding of the ice shell's composition. Any chemical  
 399 measurements of plume particles (e.g. Cassini's measurements of Enceladus' south polar  
 400 plumes using the CDA (Hansen et al., 2011; Matson et al., 2007; Waite et al., 2017)) rely  
 401 on assumptions about the origin of the particles (ocean derived or sourced from within the  
 402 shell) and the quality of chemical signatures retained from the parent reservoir. Our results  
 403 suggest that flash freezing at thermal gradients  $>100$  K/m would produce ice particles that  
 404 retain an exceptional chemical fingerprint of their parent fluid. However, if plume particles  
 405 form through a more temperate process (e.g. slow ascension through a warm fracture (e.g.  
 406 (J. Schmidt et al., 2008))) they may only preserve a fraction of the source fluid's composition.  
 407 If the thermal environment in the region of particle generation is known, our results can be  
 408 utilized to link particle chemistry observations to parent reservoir chemistry. Lastly, any  
 409 ocean-surface transport will be mediated by impurity entrainment at the ice-ocean interface  
 410 (Allu Peddinti & McNamara, 2015). Thus, constraining material entrainment rates is crucial  
 411 to assessing the fluxes associated with potential chemical overturn within the ice shell that  
 412 may facilitate disequilibrium chemistries favorable for life (Hand et al., 2007; Vance et  
 413 al., 2016) and will govern observable biosignature delivery to the surface/upper ice shell  
 414 (B. E. Schmidt, 2020).

415 Although there are important parallels between the ice-ocean interfaces of icy worlds  
 416 and those found on Earth beneath sea ice and ice shelves (e.g. (Buffo, Schmidt, Huber, &  
 417 Walker, 2020; Greeley et al., 1998; Pappalardo & Coon, 1996)), there are important facets of  
 418 their scale and structure which may facilitate unique processes not represented in terrestrial  
 419 analog systems. For Europa, the thickness of the ice shell ( $\sim 10$ - $30$  km) coupled with a  
 420 gravity approximately one tenth that of Earth ( $\sim 1.32$  m/s<sup>2</sup>) leads to predicted ice-ocean  
 421 interface mushy layer thicknesses of 537 m and 1611 m for a 10 km and 30 km thick ice

422 shell, respectively (using equation 10 and the coefficients given in the caption of Figure  
 423 5). These thicknesses far exceed the  $\sim 10\text{-}30$  cm thick mushy layers observed in sea ice  
 424 (Feltham et al., 2006; Hunke et al., 2011; Worster & Rees Jones, 2015) and meters to tens  
 425 of meters of hydraulic connectivity observed at the base of ice shelves (Craven et al., 2009;  
 426 Zotikov et al., 1980). With the likely global nature of Europa’s ice-ocean interface, and  
 427 its adjacency to the moon’s ductile, likely convective, icy mantle (Barr & McKinnon, 2007;  
 428 Han & Showman, 2005; McKinnon, 1999), we suggest that in a number of aspects it may be  
 429 best thought of as a core-mantle phase boundary, akin to the D” layer of Earth. Existing  
 430 as a multiphase layer, separating a denser fluid underlying a lighter solid (outer core and  
 431 mantle, respectively), this elusive layer plays an integral role in Earth’s geophysical evolution  
 432 (Burke et al., 2008; Maruyama et al., 2007; Olson et al., 1987). In this analogy, regional  
 433 topography and heterogeneous heat flow could drive ice dynamics mirroring diapiric mantle  
 434 plumes and tectonic processes on Earth (Burke et al., 2008; Lay et al., 2008; Olson et al.,  
 435 1987), both of which have been suggested by geomorphological observations of features on  
 436 Europa’s surface (Head et al., 1999; Kattenhorn & Hurford, 2009; Kattenhorn & Prockter,  
 437 2014; Pappalardo & Barr, 2004; Prockter et al., 2002; B. E. Schmidt et al., 2011). If this is  
 438 the case, the multiphase ice-ocean boundary of Europa not only governs the rates of heat  
 439 and mass transport between the two reservoirs via micro- and mesoscopic physics but may  
 440 also dictate regional and global scale geophysical processes. With the importance the D”  
 441 layer plays in magmatic and tectonic processes on Earth, and analogous cryovolcanism (ice  
 442 shell hydrology) (Fagents et al., 2000; Sparks et al., 2017) and ice tectonism (Kattenhorn &  
 443 Hurford, 2009; Kattenhorn & Prockter, 2014) likely occurring on Europa, constraining the  
 444 structure and heterogeneity of the ice-ocean interface mushy layer promises to provide novel  
 445 insight on the dynamics and evolution of icy worlds. Additionally, and perhaps surprisingly,  
 446 the ice-ocean interface of Europa provides a more accessible (See NASA’s SESAME project  
 447 (Howell & Pappalardo, 2020)) analog of the terrestrial D” layer and could be used to explore  
 448 hypotheses regarding the Earth’s interior.

449 The porous and reactive nature of the ice-ocean interface would provide an exceptional  
 450 niche for any biology in the oceans of icy satellites. As the location where surface derived  
 451 oxidants would be introduced into the theoretically reduced ocean (Hand et al., 2007; Vance  
 452 et al., 2016), the ice-ocean boundary layer of Europa would be rich in chemical gradients  
 453 and disequilibria in an otherwise likely oligotrophic water column (less the ocean-rock in-  
 454 terface  $\sim 100$  km below) (Lipps & Rieboldt, 2005). This is in addition to the chemical  
 455 gradients produced by ice formation (e.g. Section 3.3). On Earth, the basal surfaces of  
 456 oceanic ices (sea ice, ice shelves) house a rich community of bacteria, algae and higher order  
 457 heterotrophs (Daly et al., 2013; Gradinger et al., 1999; Loose et al., 2011; Spindler,  
 458 1994; Thomas & Dieckmann, 2003). On icy worlds, devoid of sunlight, any biotic systems  
 459 will likely be fueled by chemolithoautotrophic primary producers (Hoover & Pikuta, 2010;  
 460 Pikuta & Hoover, n.d.; B. E. Schmidt, 2020), similar to hydrothermal, deep benthic, and/or  
 461 endolithic environments on Earth. In thick ice shells with permeable layers  $>1$  km thick  
 462 there may be an array of unique ice-ocean/brine sub-environments within these layers which  
 463 could be colonized by extremophiles adapted to take advantage of regional sources of en-  
 464 ergy. With Europa’s prominence amongst high priority astrobiology targets constraining  
 465 the physicochemical dynamics and habitability of a long-lived (in comparison to shallow  
 466 features) and accessible (in comparison to the seafloor) biologically favorable niche is in line  
 467 with a multitude of NASA goals (NRC, 2012; Des Marais et al., 2008; Hendrix et al., 2019).

## 468 5 Conclusion

469 The ice-ocean interface of Europa and other icy worlds is likely characterized by a  
 470 dynamic mushy zone consisting of porous ice and saline interstitial brine. Such reactive phase  
 471 change boundaries play an integral role in both the biogeochemical cycling and geophysics  
 472 of the Earth (Loose et al., 2011; Hunke et al., 2011). Similarly, as a likely ubiquitous feature  
 473 on Europa and other icy satellites the ice-ocean interface dictates ocean-surface transport,

474 the physicochemical characteristics of the ice shell, likely governs both regional and global  
 475 geophysical processes, and may provide a gradient rich oasis for any resident organisms.  
 476 Constraining the dynamics and properties of the ice-ocean interface will improve geophysical  
 477 models of the ice shell, aid in the planning and synthesis of missions in the lens of planetary  
 478 exploration and planetary protection directives, and help constrain the habitability of ice-  
 479 ocean worlds.

## 480 Acknowledgments

481 *Data Availability Statement:* SOFTBALL and its associated documentation can be found in  
 482 (J. R. G. Parkinson, Martin, & Buffo, 2020). All model input files used in this manuscript  
 483 can be found in the repository directory 'mushy-layer/examples/europa' (J. R. G. Parkinson,  
 484 Martin, & Buffo, 2020).

## 485 References

- 486 Ackley, S. F., & Sullivan, C. W. (1994). Physical controls on the development and charac-  
 487 teristics of antarctic sea ice biological communities—a review and synthesis [Journal  
 488 Article]. *Deep Sea Research Part I: Oceanographic Research Papers*, 41(10), 1583-  
 489 1604.
- 490 Allu Peddinti, D., & McNamara, A. K. (2015). Material transport across europa’s ice shell  
 491 [Journal Article]. *Geophysical Research Letters*, 42(11), 4288-4293.
- 492 Assur, A. (1958). Composition of sea ice and its tensile strength [Journal Article]. *Arctic*  
 493 *sea ice*, 598, 106-138.
- 494 Barge, L. M., Abedian, Y., Doloboff, I. J., Nuñez, J. E., Russell, M. J., Kidd, R. D., & Kanik,  
 495 I. (2015). Chemical gardens as flow-through reactors simulating natural hydrothermal  
 496 systems [Journal Article]. *JoVE (Journal of Visualized Experiments)*(105), e53015.
- 497 Barr, A. C., & McKinnon, W. B. (2007). Convection in ice shells and mantles with  
 498 self-consistent grain size [Journal Article]. *Journal of Geophysical Research: Planets*,  
 499 112(E2).
- 500 Bierson, C. J., Nimmo, F., & Stern, S. A. (2020). Evidence for a hot start and early ocean  
 501 formation on pluto [Journal Article]. *Nature Geoscience*. Retrieved from [https://](https://doi.org/10.1038/s41561-020-0595-0)  
 502 [doi.org/10.1038/s41561-020-0595-0](https://doi.org/10.1038/s41561-020-0595-0) doi: 10.1038/s41561-020-0595-0
- 503 Brown, E. K., Buffo, J. J., Grantham, M., Pontefract, A., Glass, J., Ingall, E., ... Carr,  
 504 C. (2020). Trapped in the ice: An analysis of brines in british columbia’s hypersaline  
 505 lakes [Journal Article]. *LPI(2326)*, 2218.
- 506 Buffo, J. J. (2019). *Multiphase reactive transport in planetary ices* (Thesis). Georgia  
 507 Institute of Technology.
- 508 Buffo, J. J., Schmidt, B. E., Huber, C., & Meyer, C. R. (2020). Characterizing the ice-ocean  
 509 interface of icy worlds: A theoretical approach. *Icarus*. doi: 10.1002/essoar.10503011  
 510 .1
- 511 Buffo, J. J., Schmidt, B. E., Huber, C., & Walker, C. C. (2020). Entrainment and dynamics  
 512 of ocean-derived impurities within europa’s ice shell [Journal Article]. *JGR: Planets*.
- 513 Burke, K., Steinberger, B., Torsvik, T. H., & Smethurst, M. A. (2008). Plume generation  
 514 zones at the margins of large low shear velocity provinces on the core–mantle boundary  
 515 [Journal Article]. *Earth and Planetary Science Letters*, 265(1-2), 49-60.
- 516 Cartwright, J. H. E., Escribano, B., González, D. L., Sainz-Díaz, C. I., & Tival, I. (2013).  
 517 Brinicles as a case of inverse chemical gardens [Journal Article]. *Langmuir*, 29(25),  
 518 7655-7660.
- 519 Cartwright, J. H. E., García-Ruiz, J. M., Novella, M. L., & Otálora, F. (2002). Formation  
 520 of chemical gardens [Journal Article]. *Journal of colloid and interface science*, 256(2),  
 521 351-359.
- 522 Chivers, C. J., Buffo, J. J., & Schmidt, B. E. (2020). Thermal and chemical evolution of  
 523 small, shallow water bodies on europa [Journal Article]. *LPI(2326)*, 1047.
- 524 Cottier, F., Eicken, H., & Wadhams, P. (1999). Linkages between salinity and brine chan-

- nel distribution in young sea ice [Journal Article]. *Journal of Geophysical Research: Oceans*, 104(C7), 15859-15871.
- Craft, K. L., Patterson, G. W., Lowell, R. P., & Germanovich, L. (2016). Fracturing and flow: Investigations on the formation of shallow water sills on europa [Journal Article]. *Icarus*, 274, 297-313.
- Craven, M., Allison, I., Fricker, H. A., & Warner, R. (2009). Properties of a marine ice layer under the amery ice shelf, east antarctica [Journal Article]. *Journal of Glaciology*, 55(192), 717-728.
- Daly, M., Rack, F., & Zook, R. (2013). *Edwardsiella andrillae*, a new species of sea anemone from antarctic ice [Journal Article]. *PloS one*, 8(12), e83476.
- Des Marais, D. J., Nuth, J. A., Allamandola, L. J., Boss, A. P., Farmer, J. D., Hoehler, T. M., ... Runnegar, B. (2008). The nasa astrobiology roadmap [Journal Article]. *Astrobiology*, 8(4), 715-730.
- Di Paolo, F., Lauro, S. E., Castelletti, D., Mitri, G., Bovololo, F., Cosciotti, B., ... Bruzzone, L. (2016). Radar signal penetration and horizons detection on europa through numerical simulations [Journal Article]. *IEEE Journal of Selected Topics in Applied Earth Observations and Remote Sensing*, 10(1), 118-129.
- Dombard, A. J., Patterson, G. W., Lederer, A. P., & Prockter, L. M. (2013). Flanking fractures and the formation of double ridges on europa [Journal Article]. *Icarus*, 223(1), 74-81.
- Durham, W. B., Stern, L. A., Kubo, T., & Kirby, S. H. (2005). Flow strength of highly hydrated mg-and na-sulfate hydrate salts, pure and in mixtures with water ice, with application to europa [Journal Article]. *Journal of Geophysical Research: Planets*, 110(E12).
- Fagents, S. A., Greeley, R., Sullivan, R. J., Pappalardo, R. T., Prockter, L. M., & Team, G. S. (2000). Cryomagmatic mechanisms for the formation of rhadamanthys linea, triple band margins, and other low-albedo features on europa [Journal Article]. *Icarus*, 144(1), 54-88.
- Feltham, D. L., Untersteiner, N., Wettlaufer, J. S., & Worster, M. G. (2006). Sea ice is a mushy layer [Journal Article]. *Geophysical Research Letters*, 33(14).
- Fortes, A. D. (2000). Exobiological implications of a possible ammonia-water ocean inside titan [Journal Article]. *Icarus*, 146(2), 444-452.
- Freitag, J., & Eicken, H. (2003). Meltwater circulation and permeability of arctic summer sea ice derived from hydrological field experiments [Journal Article]. *Journal of Glaciology*, 49(166), 349-358.
- Golden, K. M., Ackley, S. F., & Lytle, V. (1998). The percolation phase transition in sea ice [Journal Article]. *Science*, 282(5397), 2238-2241.
- Golden, K. M., Eicken, H., Heaton, A. L., Miner, J., Pringle, D. J., & Zhu, J. (2007). Thermal evolution of permeability and microstructure in sea ice [Journal Article]. *Geophysical Research Letters*, 34(16).
- Gradinger, R., Friedrich, C., & Spindler, M. (1999). Abundance, biomass and composition of the sea ice biota of the greenland sea pack ice [Journal Article]. *Deep Sea Research Part II: Topical Studies in Oceanography*, 46(6-7), 1457-1472.
- Grasset, O., Dougherty, M. K., Coustenis, A., Bunce, E. J., Erd, C., Titov, D., ... Fletcher, L. N. (2013). Jupiter icy moons explorer (juice): An esa mission to orbit ganymede and to characterise the jupiter system [Journal Article]. *Planetary and Space Science*, 78, 1-21.
- Greeley, R., Sullivan, R., Coon, M. D., Geissler, P. E., Tufts, B. R., Head III, J. W., ... Moore, J. M. (1998). Terrestrial sea ice morphology: Considerations for europa [Journal Article]. *Icarus*, 135(1), 25-40.
- Hammond, N. P., Barr, A. C., & Parmentier, E. M. (2016). Recent tectonic activity on pluto driven by phase changes in the ice shell [Journal Article]. *Geophysical Research Letters*, 43(13), 6775-6782.
- Han, L., & Showman, A. P. (2005). Thermo-compositional convection in europa's icy shell with salinity [Journal Article]. *Geophysical research letters*, 32(20).

- 580 Hand, K. P., Carlson, R. W., & Chyba, C. F. (2007). Energy, chemical disequilibrium, and  
581 geological constraints on europa [Journal Article]. *Astrobiology*, *7*(6), 1006-1022.
- 582 Hand, K. P., Chyba, C., Priscu, J., Carlson, R., & Nealon, K. (2009). Astrobiology and  
583 the potential for life on europa [Journal Article]. *Europa*, 589-629.
- 584 Hand, K. P., & Chyba, C. F. (2007). Empirical constraints on the salinity of the european  
585 ocean and implications for a thin ice shell [Journal Article]. *Icarus*, *189*(2), 424-438.
- 586 Hansen, C., Shemansky, D. E., Esposito, L. W., Stewart, A., Lewis, B., Colwell, J., ...  
587 Teolis, B. (2011). The composition and structure of the enceladus plume [Journal  
588 Article]. *Geophysical Research Letters*, *38*(11).
- 589 Head, J. W., Pappalardo, R. T., & Sullivan, R. (1999). Europa: Morphological charac-  
590 teristics of ridges and triple bands from galileo data (e4 and e6) and assessment of a  
591 linear diapirism model [Journal Article]. *Journal of Geophysical Research: Planets*,  
592 *104*(E10), 24223-24236.
- 593 Hendrix, A. R., Hurford, T. A., Barge, L. M., Bland, M. T., Bowman, J. S., Brinckerhoff,  
594 W., ... Collins, G. C. (2019). The nasa roadmap to ocean worlds [Journal Article].  
595 *Astrobiology*, *19*(1), 1-27.
- 596 Hoover, R. B., & Pikuta, E. V. (2010). Psychrophilic and psychrotolerant microbial ex-  
597 tremophiles in polar environments [Journal Article].
- 598 Howell, S. M., & Pappalardo, R. T. (2018). Band formation and ocean-surface interaction  
599 on europa and ganymede [Journal Article]. *Geophysical Research Letters*, *45*(10),  
600 4701-4709.
- 601 Howell, S. M., & Pappalardo, R. T. (2020). Nasa's europa clipper—a mission to a potentially  
602 habitable ocean world [Journal Article]. *Nature Communications*, *11*(1), 1-4.
- 603 Hunke, E., Notz, D., Turner, A., & Vancoppenolle, M. (2011). The multiphase physics of sea  
604 ice: a review for model developers [Journal Article]. *The Cryosphere*, *5*(4), 989-1009.
- 605 Jia, X., Kivelson, M. G., Khurana, K. K., & Kurth, W. S. (2018). Evidence of a plume on  
606 europa from galileo magnetic and plasma wave signatures [Journal Article]. *Nature*  
607 *Astronomy*, *2*(6), 459-464.
- 608 Johnson, B. C., Sheppard, R. Y., Pascuzzo, A. C., Fisher, E. A., & Wiggins, S. E. (2017).  
609 Porosity and salt content determine if subduction can occur in europa's ice shell [Jour-  
610 nal Article]. *Journal of Geophysical Research: Planets*, *122*(12), 2765-2778.
- 611 Kalousová, K., Schroeder, D. M., & Soderlund, K. M. (2017). Radar attenuation in europa's  
612 ice shell: Obstacles and opportunities for constraining the shell thickness and its  
613 thermal structure [Journal Article]. *Journal of Geophysical Research: Planets*, *122*(3),  
614 524-545.
- 615 Kargel, J. S., Kaye, J. Z., Head III, J. W., Marion, G. M., Sassen, R., Crowley, J. K., ...  
616 Hogenboom, D. L. (2000). Europa's crust and ocean: origin, composition, and the  
617 prospects for life [Journal Article]. *Icarus*, *148*(1), 226-265.
- 618 Kattenhorn, S. A., & Hurford, T. (2009). Tectonics of europa [Book Section]. In *Europa*  
619 (p. 199-236). University of Arizona Press Tucson.
- 620 Kattenhorn, S. A., & Prockter, L. M. (2014). Evidence for subduction in the ice shell of  
621 europa [Journal Article]. *Nature Geoscience*, *7*(10), 762.
- 622 Katz, R. F., & Worster, M. G. (2008). Simulation of directional solidification, thermochem-  
623 ical convection, and chimney formation in a hele-shaw cell [Journal Article]. *Journal*  
624 *of Computational Physics*, *227*(23), 9823-9840.
- 625 Khurana, K., Kivelson, M., Stevenson, D., Schubert, G., Russell, C., Walker, R., &  
626 Polansky, C. (1998). Induced magnetic fields as evidence for subsurface oceans  
627 in europa and callisto [Journal Article]. *Nature*, *395*(6704), 777.
- 628 Lay, T., Hernlund, J., & Buffett, B. A. (2008). Core–mantle boundary heat flow [Journal  
629 Article]. *Nature geoscience*, *1*(1), 25.
- 630 Le Bars, M., & Worster, M. G. (2006). Interfacial conditions between a pure fluid and a  
631 porous medium: implications for binary alloy solidification [J. Fluid Mech.].
- 632 Lipps, J. H., & Rieboldt, S. (2005). Habitats and taphonomy of europa [Journal Article].  
633 *Icarus*, *177*(2), 515-527.
- 634 Loose, B., Miller, L. A., Elliott, S., & Papakyriakou, T. (2011). Sea ice biogeochemistry and

- 635 material transport across the frozen interface [Journal Article]. *Oceanography*, 24(3),  
636 202-218.
- 637 Mahadevan, K. (2017). *The growth and dynamics of brinicles* (Uundergraduate Thesis).  
638 School of Engineering and Applied Sciences, Harvard University.
- 639 Manga, M., & Michaut, C. (2017). Formation of lenticulae on europa by saucer-shaped sills  
640 [Journal Article]. *Icarus*, 286, 261-269.
- 641 Marion, G. M., Fritsen, C. H., Eicken, H., & Payne, M. C. (2003). The search for life  
642 on europa: limiting environmental factors, potential habitats, and earth analogues  
643 [Journal Article]. *Astrobiology*, 3(4), 785-811.
- 644 Maruyama, S., Santosh, M., & Zhao, D. (2007). Superplume, supercontinent, and post-  
645 perovskite: mantle dynamics and anti-plate tectonics on the core–mantle boundary  
646 [Journal Article]. *Gondwana Research*, 11(1-2), 7-37.
- 647 Matson, D. L., Castillo, J. C., Lumine, J., & Johnson, T. V. (2007). Enceladus' plume:  
648 Compositional evidence for a hot interior [Journal Article]. *Icarus*, 187(2), 569-573.
- 649 McCarthy, C., Blackford, J., & Jeffree, C. (2013). Low-temperature-sem study of dihedral  
650 angles in the ice-i/sulfuric acid partially molten system [Journal Article]. *Journal of*  
651 *microscopy*, 249(2), 150-157.
- 652 McCarthy, C., Cooper, R. F., Goldsby, D. L., Durham, W. B., & Kirby, S. H. (2011). Tran-  
653 sient and steady state creep response of ice i and magnesium sulfate hydrate eutectic  
654 aggregates [Journal Article]. *Journal of Geophysical Research: Planets*, 116(E4).
- 655 McCarthy, C., Cooper, R. F., Kirby, S. H., Rieck, K. D., & Stern, L. A. (2007). Solidifica-  
656 tion and microstructures of binary ice-i/hydrate eutectic aggregates [Journal Article].  
657 *American Mineralogist*, 92(10), 1550-1560.
- 658 McKinnon, W. B. (1999). Convective instability in europa's floating ice shell [Journal  
659 Article]. *Geophysical Research Letters*, 26(7), 951-954.
- 660 McKinnon, W. B., & Kirk, R. L. (2014). Triton [Book Section]. In *Encyclopedia of the*  
661 *solar system* (p. 861-881). Elsevier.
- 662 Michaut, C., & Manga, M. (2014). Domes, pits, and small chaos on europa produced  
663 by water sills [Journal Article]. *Journal of Geophysical Research: Planets*, 119(3),  
664 550-573.
- 665 Moore, J. C. (2000). Models of radar absorption in european ice [Journal Article]. *Icarus*,  
666 147(1), 292-300.
- 667 Nimmo, F. (2020). Solving the puzzle of enceladus's active south pole [Journal Article].  
668 *Proceedings of the National Academy of Sciences*, 117(28), 16107-16108.
- 669 Nimmo, F., & Pappalardo, R. (2016). Ocean worlds in the outer solar system [Journal  
670 Article]. *Journal of Geophysical Research: Planets*, 121(8), 1378-1399.
- 671 NRC. (2012). *Vision and voyages for planetary science in the decade 2013-2022* [Book].  
672 National Academies Press.
- 673 Olson, P., Schubert, G., & Anderson, C. (1987). Plume formation in the d " -layer and the  
674 roughness of the core–mantle boundary [Journal Article]. *Nature*, 327(6121), 409.
- 675 Pappalardo, R. T., & Barr, A. C. (2004). The origin of domes on europa: The role of  
676 thermally induced compositional diapirism [Journal Article]. *Geophysical Research*  
677 *Letters*, 31(1).
- 678 Pappalardo, R. T., & Coon, M. (1996). A sea ice analog for the surface of europa [Conference  
679 Proceedings]. In *Lunar and planetary science conference* (Vol. 27).
- 680 Pappalardo, R. T., Senske, D., Korth, H., Klima, R., Vance, S., & Craft, K. (2017). The  
681 europa clipper mission: Exploring the habitability of a unique icy world [Conference  
682 Proceedings]. In *European planetary science congress* (Vol. 11).
- 683 Parkinson, C. D., Liang, M.-C., Yung, Y. L., & Kirschvink, J. L. (2008). Habitability of  
684 enceladus: planetary conditions for life [Journal Article]. *Origins of Life and Evolution*  
685 *of Biospheres*, 38(4), 355-369.
- 686 Parkinson, J. R. G. (2019). *Nonlinear convection in sea ice and other mushy layers* (Thesis).  
687 University of Oxford.
- 688 Parkinson, J. R. G., Martin, D., & Buffo, J. (2020, October). *jrgparkinson/mushy-layer:*  
689 *Code and input files for Europa simulations*. Zenodo. Retrieved from <https://doi>

- 690 .org/10.5281/zenodo.4118549 doi: 10.5281/zenodo.4118549
- 691 Parkinson, J. R. G., Martin, D. F., Wells, A. J., & Katz, R. F. (2020). Modelling bi-  
 692 nary alloy solidification with adaptive mesh refinement [Journal Article]. *Journal of*  
 693 *Computational Physics: X*, 5, 100043.
- 694 Petrich, C., Langhorne, P. J., & Sun, Z. F. (2006). Modelling the interrelationships between  
 695 permeability, effective porosity and total porosity in sea ice [Journal Article]. *Cold*  
 696 *Regions Science and Technology*, 44(2), 131-144.
- 697 Pikuta, E. V., & Hoover, R. B. (n.d.). Astrobiological significance of chemolithoautotrophic  
 698 acidophiles [Conference Proceedings]. In *Instruments, methods, and missions for as-*  
 699 *trobiology vii* (Vol. 5163, p. 179-190). International Society for Optics and Photonics.
- 700 Porco, C., Helfenstein, P., Thomas, P., Ingersoll, A., Wisdom, J., West, R., . . . Roatsch, T.  
 701 (2006). Cassini observes the active south pole of enceladus [Journal Article]. *science*,  
 702 311(5766), 1393-1401.
- 703 Prockter, L. M., Head, J. W., Pappalardo, R. T., Sullivan, R. J., Clifton, A. E., Giese, B.,  
 704 . . . Neukum, G. (2002). Morphology of european bands at high resolution: A mid-  
 705 ocean ridge-type rift mechanism [Journal Article]. *Journal of Geophysical Research:*  
 706 *Planets*, 107(E5).
- 707 Rees Jones, D. W., & Worster, M. G. (2013). A simple dynamical model for gravity drainage  
 708 of brine from growing sea ice [Journal Article]. *Geophysical Research Letters*, 40(2),  
 709 307-311.
- 710 Rudolph, M. L., & Manga, M. (2009). Fracture penetration in planetary ice shells [Journal  
 711 Article]. *Icarus*, 199(2), 536-541.
- 712 Santibáñez, P. A., Michaud, A. B., Vick-Majors, T. J., D'Andrilli, J., Chiuchiolo, A., Hand,  
 713 K. P., & Priscu, J. C. (2019). Differential incorporation of bacteria, organic matter,  
 714 and inorganic ions into lake ice during ice formation [Journal Article]. *Journal of*  
 715 *Geophysical Research: Biogeosciences*.
- 716 Schmidt, B. E. (2020). The astrobiology of europa and the jovian system [Journal Article].  
 717 *Planetary Astrobiology*, 185.
- 718 Schmidt, B. E., Blankenship, D., Patterson, G., & Schenk, P. (2011). Active formation  
 719 of 'chaos terrain' over shallow subsurface water on europa [Journal Article]. *Nature*,  
 720 479(7374), 502.
- 721 Schmidt, B. E., Buffo, J., & Main Campus, A. (n.d.). Biomarker production and preservation  
 722 on europa [Conference Proceedings]. In *European planetary science congress* (Vol. 11).
- 723 Schmidt, J., Brilliantov, N., Spahn, F., & Kempf, S. (2008). Slow dust in enceladus' plume  
 724 from condensation and wall collisions in tiger stripe fractures [Journal Article]. *Nature*,  
 725 451(7179), 685-688.
- 726 Schroeder, D. M., Romero-Wolf, A., Carrer, L., Grima, C., Campbell, B. A., Kofman, W.,  
 727 . . . Blankenship, D. D. (2016). Assessing the potential for passive radio sounding of  
 728 europa and ganymede with rime and reason [Journal Article]. *Planetary and Space*  
 729 *Science*, 134, 52-60.
- 730 Schubert, G., Anderson, J., Spohn, T., & McKinnon, W. (2004). Interior composition,  
 731 structure and dynamics of the galilean satellites [Journal Article]. *Jupiter: The planet,*  
 732 *satellites and magnetosphere*, 1, 281-306.
- 733 Soderlund, K. M. (2019). Ocean dynamics of outer solar system satellites [Journal Article].  
 734 *Geophysical Research Letters*, 46(15), 8700-8710. Retrieved from <GotoISI>://WOS:  
 735 000483812500013 doi: 10.1029/2018gl081880
- 736 Soderlund, K. M., Schmidt, B. E., Wicht, J., & Blankenship, D. D. (2014). Ocean-driven  
 737 heating of europa's icy shell at low latitudes [Journal Article]. *Nature Geoscience*, 7(1),  
 738 16-19. Retrieved from <GotoISI>://WOS:000328962700012 doi: 10.1038/Ngeo2021
- 739 Sotin, C., Head III, J. W., & Tobie, G. (2002). Europa: Tidal heating of upwelling thermal  
 740 plumes and the origin of lenticulae and chaos melting [Journal Article]. *Geophysical*  
 741 *Research Letters*, 29(8), 74-1-74-4.
- 742 Sparks, W. B., Hand, K., McGrath, M., Bergeron, E., Cracraft, M., & Deustua, S. (2016).  
 743 Probing for evidence of plumes on europa with hst/stis [Journal Article]. *The Astro-*  
 744 *physical Journal*, 829(2), 121.

- 745 Sparks, W. B., Schmidt, B. E., McGrath, M. A., Hand, K. P., Spencer, J. R., Cracraft,  
746 M., & Deustua, S. E. (2017). Active cryovolcanism on europa? [Journal Article]. *The*  
747 *Astrophysical Journal Letters*, *839*(2), L18.
- 748 Spaun, N., Head, J., Collins, G., Prockter, L., & Pappalardo, R. (1998). Conamara chaos  
749 region, europa: Reconstruction of mobile polygonal ice blocks [Journal Article]. *Geo-*  
750 *physical research letters*, *25*(23), 4277-4280.
- 751 Spindler, M. (1994). Notes on the biology of sea ice in the arctic and antarctic [Journal  
752 Article]. *Polar Biology*, *14*(5), 319-324.
- 753 Steefel, C. I., DePaolo, D. J., & Lichtner, P. C. (2005). Reactive transport modeling: An  
754 essential tool and a new research approach for the earth sciences [Journal Article].  
755 *Earth and Planetary Science Letters*, *240*(3-4), 539-558.
- 756 Tedesco, L., & Vichi, M. (2014). Sea ice biogeochemistry: A guide for modellers [Journal  
757 Article]. *PloS one*, *9*(2), e89217.
- 758 Thomas, D. N., & Dieckmann, G. S. (2003). Biogeochemistry of antarctic sea ice [Book  
759 Section]. In *Oceanography and marine biology, an annual review, volume 40* (p. 151-  
760 156). CRC Press.
- 761 Thomas, D. N., & Dieckmann, G. S. (2008). *Sea ice: an introduction to its physics,*  
762 *chemistry, biology and geology* [Book]. John Wiley & Sons.
- 763 Trumbo, S. K., Brown, M. E., & Hand, K. P. (2019). Sodium chloride on the surface of  
764 europa [Journal Article]. *Science advances*, *5*(6), eaaw7123.
- 765 Vance, S. D., Barge, L. M., Cardoso, S. S., & Cartwright, J. H. (2019). Self-assembling  
766 ice membranes on europa: Brinicle properties, field examples, and possible energetic  
767 systems in icy ocean worlds [Journal Article]. *arXiv preprint arXiv:1903.01584*.
- 768 Vance, S. D., & Brown, J. M. (2013). Thermodynamic properties of aqueous  $\text{mgso}_4$  to  
769 800 mpa at temperatures from -20 to 100° c and concentrations to 2.5 mol  $\text{kg}^{-1}$  from  
770 sound speeds, with applications to icy world oceans [Journal Article]. *Geochimica et*  
771 *Cosmochimica Acta*, *110*, 176-189.
- 772 Vance, S. D., Hand, K. P., & Pappalardo, R. T. (2016). Geophysical controls of chemical  
773 disequilibria in europa [Journal Article]. *Geophysical Research Letters*, *43*(10), 4871-  
774 4879.
- 775 Waite, J. H., Glein, C. R., Perryman, R. S., Teolis, B. D., Magee, B. A., Miller, G., ...  
776 Bouquet, A. (2017). Cassini finds molecular hydrogen in the enceladus plume: evidence  
777 for hydrothermal processes [Journal Article]. *Science*, *356*(6334), 155-159.
- 778 Walker, C., Schmidt, B., & Bassis, J. (2014). Breaking the ice: On the application of  
779 fracture system mechanics and fragmentation theory to the chaos regions of europa  
780 [Journal Article]. *LPI(1777)*, 2659.
- 781 Wells, A. J., Hitchen, J. R., & Parkinson, J. R. (2019). Mushy-layer growth and convection,  
782 with application to sea ice [Journal Article]. *Philosophical Transactions of the Royal*  
783 *Society A*, *377*(2146), 20180165.
- 784 Wells, A. J., Wettlaufer, J., & Orszag, S. (2011). Brine fluxes from growing sea ice [Journal  
785 Article]. *Geophysical Research Letters*, *38*(4).
- 786 Wettlaufer, J., Worster, M. G., & Huppert, H. E. (1997). Natural convection during  
787 solidification of an alloy from above with application to the evolution of sea ice [Journal  
788 Article]. *Journal of fluid mechanics*, *344*, 291-316.
- 789 Worster, M. G. (1991). Natural convection in a mushy layer [Journal Article]. *Journal of*  
790 *fluid mechanics*, *224*, 335-359.
- 791 Worster, M. G. (1997). Convection in mushy layers [Journal Article]. *Annual Review of*  
792 *Fluid Mechanics*, *29*(1), 91-122.
- 793 Worster, M. G., & Rees Jones, D. W. (2015). Sea-ice thermodynamics and brine drainage  
794 [Journal Article]. *Philosophical Transactions of the Royal Society A: Mathematical,*  
795 *Physical and Engineering Sciences*, *373*(2045), 20140166.
- 796 Zolotov, M. Y., & Kargel, J. (2009). *On the chemical composition of europa's icy shell,*  
797 *ocean, and underlying rocks* (Vol. 431) [Book]. University of Arizona Press Tucson,  
798 AZ.
- 799 Zolotov, M. Y., & Shock, E. L. (2001). Composition and stability of salts on the surface

800 of europa and their oceanic origin [Journal Article]. *Journal of Geophysical Research:*  
801 *Planets*, 106(E12), 32815-32827.  
802 Zotikov, I. A., Zagorodnov, V. S., & Raikovsky, J. V. (1980). Core drilling through the ross  
803 ice shelf (antarctica) confirmed basal freezing [Journal Article]. *Science*, 207(4438),  
804 1463-1465.